Progress In Electromagnetics Research C, Vol. 122, 67–82, 2022

High Isolation Four-Port Wrench Shaped Compact UWB MIMO Antenna for 3.1–10.6 GHz Band

Tangirala Gayatri[1, *], Garikipati Srinivasu[1], Durbhakula M. K. Chaitanya[2], and Virendra K. Sharma[3]

Abstract—This present article reports a high isolation four-port Wrench shaped compact UWB MIMO antenna with a novel decoupling network in the ground plane, and its step-by-step evolution is presented for 3.1–10.6 GHz. The proposed four-port MIMO antenna is fabricated on an FR4 substrate of size $44 \times 44\,\text{mm}^2$ ($0.342\lambda_0 \times 0.342\lambda_0$), where λ_0 is a free space wavelength at 2.33 GHz, with 7 mm edge-to-edge spacing between the radiating elements. It consists of four orthogonal symmetrically placed identical radiating elements each of which has a Wrench-shaped circular patch with a rectangular slot cut in the partial ground. The performance characteristics of this MIMO antenna are reflection coefficients $S_{11} \leq -10$ dB in the range from 2.33 GHz to 11.7 GHz, mutual coupling coefficients $S_{21} \leq -28.24$ dB, and $S_{31} \leq -22.35$ dB. The maximum peak gain is 5.15 dBi at 9.2 GHz, and minimum is 1.27 dBi at 3.1 GHz. The maximum efficiency is 98% at 4.66 GHz, and the minimum is 93% at 6 GHz. The diversity parameters of proposed four-port MIMO antenna are reported as ECC ≤ 0.2, DG ≤ 10, TARC ≤ -10 dB, the ratio of MEG between any two elements is near unity, and CCL < 0.38 bits/s/Hz in the band of interest. The design is fabricated and measured. The measured and simulated results are in good agreement and are within the permissible limits.

1. INTRODUCTION

In a ultra-wideband (UWB) system, it is the greatest challenge to improve the quality of communication and enhance the channel capacity. Multiple-input multiple-output (MIMO) antennas found their place as a good solution to the above issue. However, the MIMO development is very complex as it needs < -15 dB isolation between the radiating elements. The other challenges of MIMO are acquiring a low envelope correlation coefficient (ECC), high diversity gain (DG), stable total active reflection coefficient (TARC), low channel capacity loss (CCL), and unity mean effective gain (MEG) ratio. So, to improve the performance of the UWB system, the two technologies are combined to give rise to a new system called UWB MIMO. The diversity feature of MIMO uses two or more antennas to transmit or receive signals through different propagation paths so that multipath interference is minimized. Different types of diversities are spatial diversity, polarization diversity, transmitting or receiving diversity, and pattern diversity. The channel capacity of the UWB system is linearly proportional to bandwidth and signal-to-noise ratio (SNR), given by the Shannon Hartley formula (1).

$$C = B \times \log_2\left(1 + \frac{S}{N}\right) \tag{1}$$

This relationship in turn suggests that the data rate is enhanced rapidly by improving the channel capacity. The increase of bandwidth increases noise, thereby SNR decreases which in turn reduces the

Received 26 May 2022, Accepted 20 July 2022, Scheduled 4 August 2022
* Corresponding author: Tangirala Gayatri (t.gayatrihyd@gmail.com).
[1] Department of Electronics and Communications Engineering, Bhagwant University, Ajmer, India. [2] Department of Electronics and Communications Engineering, Vasavi College of Engineering, Hyderabad, India. [3] Department of Electrical and Electronics Engineering, Bhagwant University, Ajmer, India.

channel capacity. MIMO technology resolves this issue [1] by using formula (2).

$$C = B \times \log_2 \left(1 + T \times R \times \frac{S}{N}\right) \tag{2}$$

where,

C = Capacity of the channel in bits/sec;

B = Bandwidth of the channel in Hz;

T = Transmitting antennas;

R = Receiving antennas;

S = Power of the information signal;

N = Power of the noise.

From formula (2), if the number of transmitters and receivers increases, then channel capacity increases; in turn size also increases. Hence, a compromise is needed between antenna size and performance metrics. This is possible with good optimization techniques.

2. LITERATURE REVIEW

In the literature, numerous articles are available on UWB MIMO antennas. However, many of them do not cover the entire Federal Communications Commission (FCC) proposed UWB range, i.e., 3.1–10.6 GHz. Some of these designs have larger dimensions. These designs addressed mutual coupling reduction in different ways. Mutual coupling is defined as the power absorbed by the neighboring radiator when another one operates. This alters the reflection coefficients, input impedance, and radiation patterns. To reduce this mutual coupling, various mutual coupling (MC) reduction or decoupling, or isolation enhancement techniques were introduced in the literature. They are neutralization line (NL) [2], decoupling network (DN) [3–6], metasurface, metamaterial (MTM) [7], electronic band gap (EBG) [8, 9], frequency selective surface (FSS), photonic band gap (PBG), optically transparent structures [10], split ring resonator (SRR), complementary split ring resonator (CSRR) [11, 12], dielectric resonator antenna (DRA), ground plane modification (GPM), defected ground structure (DGS) [13, 14], slots [15–18], band notching techniques implementation, parasitic elements, metal strips, shorting pins, insertion of stubs [19–21], frequency reconfigurable [22, 23], implementing PIN diodes, microstrip open loop resonator (MOLR), quasi self complementary antenna (QSCA) [24], inter element spacing [25–29], insertion of slits, fractal structures, modified substrates, locating antennas on different substrate layers, etc. These techniques improve impedance matching, enhance gain, efficiency, and increase the complexity of antenna design. However, some of the decoupling techniques also reduce the antenna size. The main reason for poor isolation is that the ports of different antennas have a common ground or shared ground. The currents are coupled across ports through the shared ground which increases the coupling between these ports. Hence for isolation enhancement and to achieve greater efficiencies, mutual coupling reduction techniques must be implemented between antenna elements.

3. ANALYSIS AND DESIGN EVOLUTION OF FOUR-PORT UWB MIMO

Initially, single element compact Wrench shaped UWB monopole was implemented. Later, all possible combinations like parallel, orthogonal, and opposite manner 2×2 MIMO antennas were examined. Finally, a four-port MIMO antenna is implemented by placing elements in an orthogonally symmetric manner with different inter-elements spacing simulated. It is observed that the design with 7 mm inter-element spacing provided optimum results. This design is then verified with various decoupling networks in the ground for the enhancement of performance and improvement of isolation between the elements. It is observed that the design with a decoupling network C in the ground plane showed the optimum simulation results and good diversity performance. Hence, it is finalized for fabrication and measurement. The step-by-step evolution process of the proposed four-port UWB MIMO antenna is discussed in the following subsections.

3.1. Single Element Wrench Shaped Antenna

Figure 1 shows the design of a Wrench shaped compact UWB antenna [30] for 3.1–10.6 GHz. The antenna was fabricated on an FR4 substrate ($20 \times 17 \times 1.6\,\text{mm}^3$). It is developed by using the equation in (3) by taking feed gap (p) = 0.14 cm, constant (k) = 1.15, lower cut-off frequency (f_l) = 4.08 GHz, then the radius of patch is obtained as (a) = 6.2 mm

$$a = \left[\frac{3.2\,\text{GHz}}{f_l \times k}\right]\left[\frac{4 \times p}{9}\right] \tag{3}$$

The dimensions are achieved by applying various optimization techniques. They are substrate length (L) × width (W) = 20 mm ×17 mm, thickness of substrate = 1.6 mm, ground center rectangular slot length × width = 3 mm × 3.1 mm, partial ground length × width = 4.9 mm × 17 mm, feed line length × width = 6.32 mm × 3 mm, thickness of patch = 0.035 mm, Wrench-shaped patch radius = 6.2 mm, patch slot length × width = 3 mm × 4 mm.

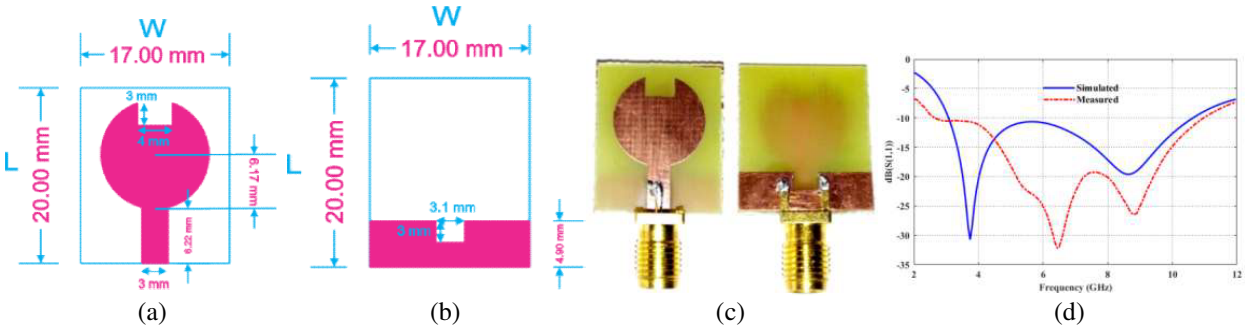

Figure 1. Compact Wrench shaped design. (a) Top layer. (b) Bottom layer. (c) Fabricated prototype. (d) Return loss characteristics.

The single element shows a VSWR ≤ 1.91, impedance bandwidth (IBW) from 3.08 GHz to 10.62 GHz, maximum peak gain as 4.9 dBi at 10.6 GHz, and the highest radiation efficiency as 98% at 7.93 GHz.

3.2. Development of Four-Port UWB MIMO Antenna without Decoupling Network

The four-port MIMO design evolution is mainly achieved by focusing on the placement of elements in an orthogonally symmetric manner with different inter-elements spacings. For 0 mm edge to edge spacing (d) between the elements, the size of MIMO antenna is $37 \times 37 \times 1.6\,\text{mm}^3$; for 3 mm, the size of MIMO antenna is $40 \times 40 \times 1.6\,\text{mm}^3$; for 5 mm, the size of MIMO antenna is $42 \times 42 \times 1.6\,\text{mm}^3$; for 7 mm, the size of MIMO antenna is $44 \times 44 \times 1.6\,\text{mm}^3$. Finally, better characteristics are observed at this stage. Ideally, the spacing between the elements should be in the range $\lambda/4 \leq d \leq \lambda/2$ apart to achieve good results. So, the further increment of inter-element spacing leads to the large size of the antenna. Hence, the design shown in Figure 4 is further examined with various decoupling networks in the ground. Section 3.3 focuses on the further evolution of this design. Figure 2 shows the structure of MIMO antenna with edge-to-edge spacing (d) between the elements.

According to arrangement symmetry of radiating elements $S_{11} = S_{22} = S_{33} = S_{44}$; $S_{21} = S_{12} = S_{32} = S_{23} = S_{43} = S_{34} = S_{41} = S_{14}$; similarly $S_{31} = S_{13} = S_{42} = S_{24}$. Hence for simplicity, S_{11}, S_{21}, S_{31} characteristics are shown in the paper at every stage of evolution. The reflection coefficients and mutual coupling coefficients comparison graphs for $d = 0, 3, 5, 7$ mm edge to edge spacing are shown in Figure 3.

From Figure 3 and Table 1, $d = 7$ mm edge-to-edge spacing only achieved the required wideband. Table 1 shows the performance characteristics of four-port MIMO antenna with a different edge-to-edge spacing without a decoupling network.

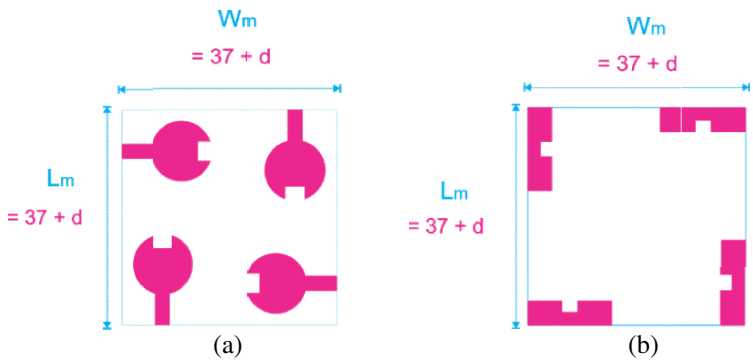

Figure 2. Four-port MIMO design with inter elements spacing 'd'. (a) Top layer. (b) Bottom layer.

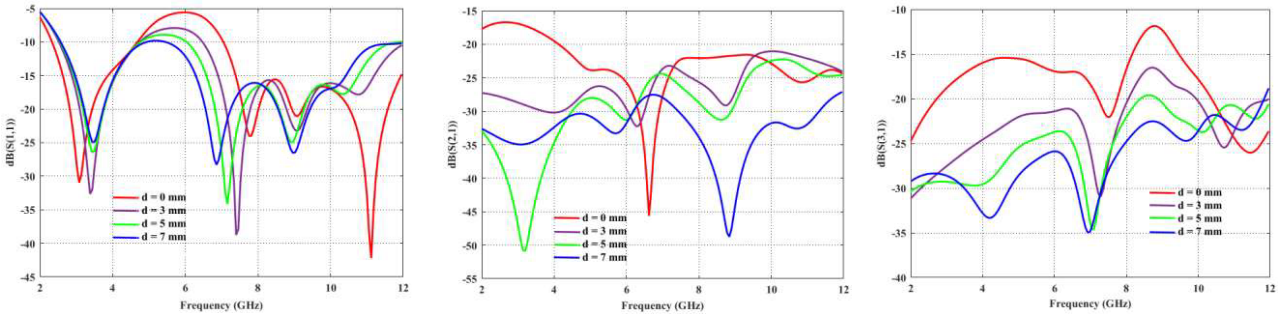

Figure 3. The comparison graphs for $d = 0, 3, 5, 7$ mm. (a) Reflection coefficients (S_{11}). (b) Mutual coupling coefficients (S_{21}). (c) Mutual coupling coefficients (S_{31}).

Table 1. Performance characteristics of four-port MIMO with different edge to edge spacing without decoupling network.

Edge to edge spacing 'd' (mm)	Size of MIMO (mm^3)	Substrate	Bandwidth (GHz)	Gain (dBi)	Isolation S_{21} (dB)	Isolation S_{31} (dB)	Max. Radiation Efficiency (%)
0	$37 \times 37 \times 1.6$	FR4	7–12	4.8	< -18.5	< -13	96
3	$40 \times 40 \times 1.6$	FR4	6.47–12	5.8	< -21.27	< -16.77	95
5	$42 \times 42 \times 1.6$	FR4	6–11.85	5.3	< -23	< -19.82	95
7	$\mathbf{44 \times 44 \times 1.6}$	**FR4**	**4.9–12**	**4.6**	$\mathbf{< -26.5}$	$\mathbf{< -21.45}$	**96**

3.3. Development of Four-Port UWB MIMO Antenna with Decoupling Network

Figure 4 shows the design with edge-to-edge spacing of 7 mm between the elements. From Section 3.2 it is observed that this design with size $44 \times 44 \times 1.6\,mm^3$ provided wideband characteristics without decoupling network.

The presented design shown in Figure 4 is now verified with three different novel decoupling networks in the ground plane for the further enhancement of impedance bandwidth to achieve FCC proposed UWB and improvement of isolation between the elements. They are shown in Figure 5.

The reflection coefficient and mutual coupling coefficients comparison graphs for the three decoupling networks are shown in Figure 6. Table 2 shows the performance characteristics of four-

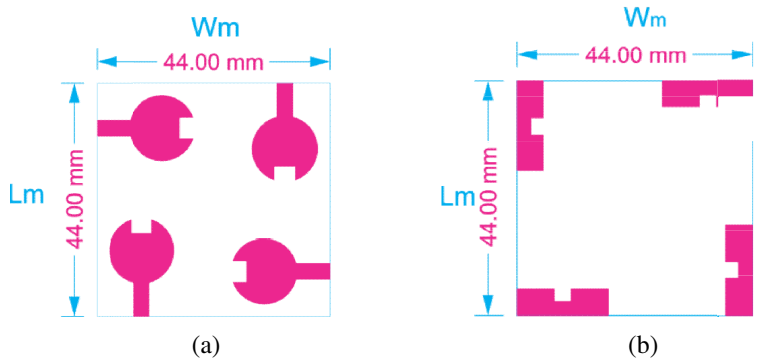

Figure 4. Four-port MIMO design with edge to edge spacing of 7 mm. (a) Top layer. (b) Bottom layer.

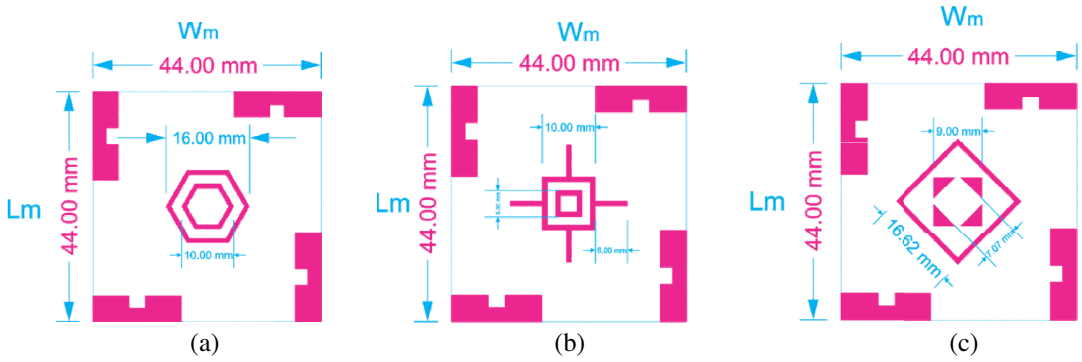

Figure 5. Decoupling structures in the ground plane. (a) Network A. (b) Network B. (c) Network C.

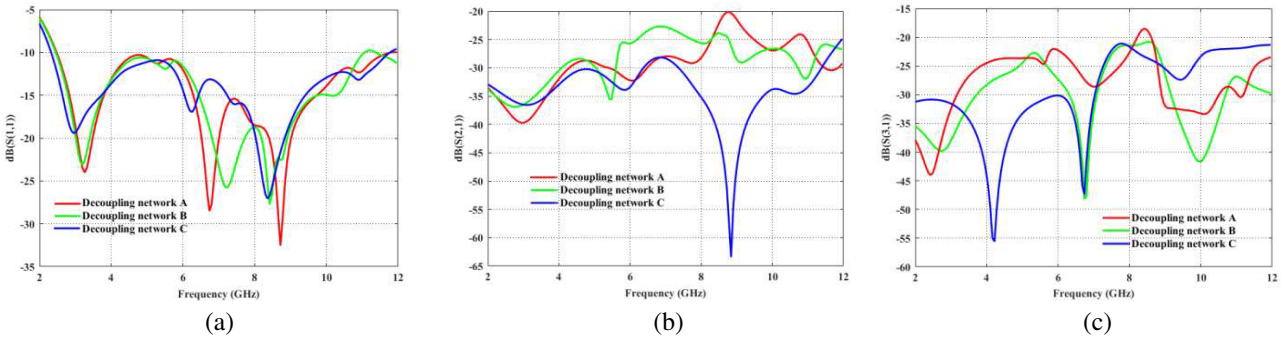

Figure 6. The comparison plots for four-port MIMO antenna with decoupling networks A, B, and C are (a) Reflection coefficients (S_{11}). (b) Mutual coupling coefficients (S_{21}). (c) Mutual coupling coefficients (S_{31}).

port MIMO antenna with three decoupling networks.

The decoupling networks also produced the following results. That is, by the introduction of network A the design achieved maximum $S_{11} = -32.13$ dB at 8.72 GHz, $S_{21} = -39.66$ dB at 3.4 GHz, and $S_{31} = -43.73$ dB at 2.4 GHz. By the introduction of network B, the design produced maximum $S_{11} = -27.11$ dB at 8.4 GHz, $S_{21} = -36.74$ dB at 2.7 GHz, and $S_{31} = -48.14$ dB at 6.74 GHz. By the introduction of network C, the design attained maximum $S_{11} = -26.93$ dB at 8.34 GHz, $S_{21} = -63.7$ dB at 8.8 GHz, and $S_{31} = -55.63$ dB at 4.2 GHz. From these results and Table 2, it is observed that the four-port MIMO design shown in Figure 4 achieved desired performance characteristics in the required band of interest for all three decoupling networks A, B, C shown in Figure 5. But the design with decoupling network C achieved good performance compared to other decoupling networks.

Table 2. Performance characteristics of four-port MIMO antenna with three decoupling networks.

Decoupling structure	Size of MIMO (mm^3)	Substrate	Bandwidth (GHz)	Gain (dBi)	Isolation S_{21} (dB)	Isolation S_{31} (dB)	Max. Radiation Efficiency (%)
A	$44 \times 44 \times 1.6$	FR4	2.48–11.5	5	< -20	< -18.5	95
B	$44 \times 44 \times 1.6$	FR4	2.46–11	4.8	< -22.61	< -20.85	96
C	$\mathbf{44 \times 44 \times 1.6}$	**FR4**	**2.33–11.7**	**5.15**	$\mathbf{< -28.24}$	$\mathbf{< -22.35}$	**98**

3.4. Proposed Four-Port MIMO Design with Step by Step Evolution of Decoupling Network C

The four-port MIMO design shown in Figure 4 is fabricated with decoupling network C shown in Figure 5(c). The performance characteristics of the proposed four-port MIMO design with step-by-step evolution of decoupling network C are shown in Figure 7 and listed in Table 3.

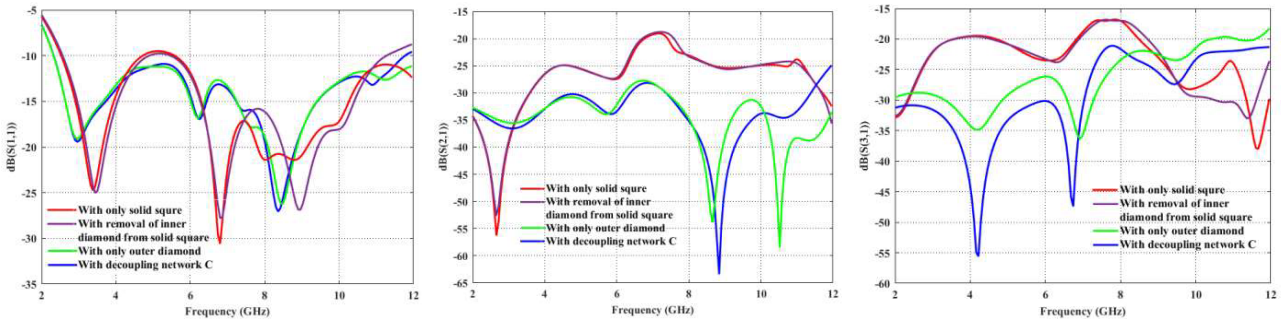

(a) (b) (c)

Figure 7. The comparison plots for proposed four-port MIMO antenna with step by step evolution of decoupling network C. (a) Reflection coefficients (S_{11}). (b) Mutual coupling coefficients (S_{21}). (c) Mutual coupling coefficients (S_{31}).

Table 3. Performance characteristics of proposed four-port MIMO antenna with step by step evolution of decoupling network C.

Decoupling Structure	Size of MIMO (mm^3)	Substrate	Bandwidth (GHz)	Gain (dBi)	Isolation S_{21} (dB)	Isolation S_{31} (dB)	Max. Radiation Efficiency (%)
With solid square	$44 \times 44 \times 1.6$	FR4	5.58–12	3.75	< -18.83	< -16.76	95
With removal of inner diamond from solid square	$44 \times 44 \times 1.6$	FR4	5.45–11.27	4.4	< -26	< -22.25	95
With outer diamond	$44 \times 44 \times 1.6$	FR4	3.32–12	4.23	< -27.32	< -19.81	94
With decoupling network C	$\mathbf{44 \times 44 \times 1.6}$	**FR4**	**2.33–11.7**	**5.15**	$\mathbf{< -28.24}$	$\mathbf{< -22.35}$	**98**

From Figure 7 it is observed that the proposed four-port MIMO design performed well with better isolation characteristics and good diversity performance only in the final stage of evolution of decoupling network C. Hence, the structure with decoupling network C is fabricated and measured.

4. PROPOSED FOUR-PORT UWB MIMO RESULTS AND DISCUSSION

The simulated and measured results of the proposed four-port MIMO design such as S parameters, radiation patterns, current distribution, peak gain, and radiation efficiency are discussed here. The various diversity performance parameters are discussed in Section 5.

4.1. Fabricated Prototype and Measurement of Proposed Four-Port MIMO Design

Figure 8 shows the fabricated prototype of the proposed four-port MIMO design and measurement in an anechoic chamber.

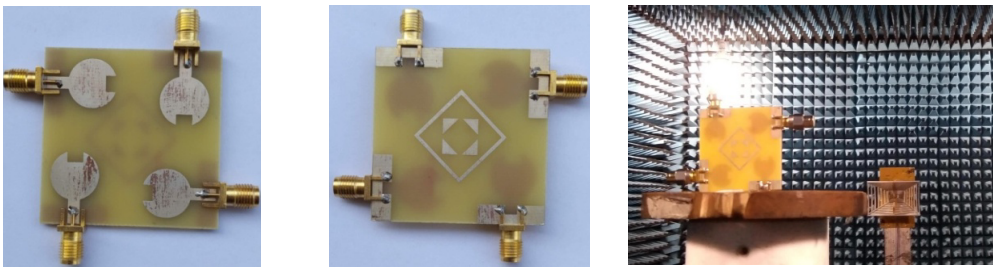

(a) (b) (c)

Figure 8. Fabricated prototype of proposed four-port MIMO with decoupling network C. (a) Top view. (b) Bottom view. (c) Measurement in anechoic chamber.

The MIMO performance in terms of reflection coefficients, transmission coefficients, mutual coupling coefficients, peak gain, radiation efficiency, 2D radiation pattern, ECC, and DG are measured.

4.2. Reflection and Transmission Coefficients

The fabricated four-port MIMO S parameters are measured using Vector Network Analyzer (VNA) and compared with the simulated results. Figure 9 shows the comparison between simulated and measured S parameters. According to arrangement symmetry of radiating elements $S_{11} = S_{22} = S_{33} = S_{44}$; and $S_{21} = S_{12} = S_{32} = S_{23} = S_{43} = S_{34} = S_{41} = S_{14}$; similarly $S_{31} = S_{13} = S_{42} = S_{24}$. Hence for simplicity, S_{11}, S_{21}, S_{31} characteristics are shown in the following figures.

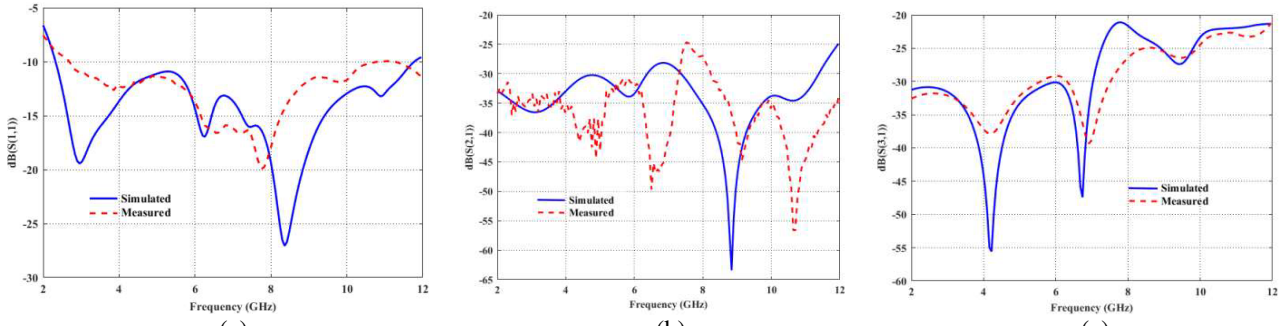

(a) (b) (c)

Figure 9. Comparison plots of fabricated four-port MIMO antenna. (a) Reflection coefficients (S_{11}). (b) Mutual coupling coefficients (S_{21}). (c) Mutual coupling coefficients (S_{31}).

Figure 9 shows that reflection coefficients $S_{11} \leq -10\,\text{dB}$ in the range 2.33 GHz to 11.7 GHz, mutual coupling coefficients $S_{21} \leq -28.24\,\text{dB}$, $S_{31} \leq -22.35\,\text{dB}$. The measured and simulated results are in good agreement over the band of interest 3.1–10.6 GHz.

4.3. Surface Current Distribution

Surface current distribution is verified with excited port 1, and the remaining ports are terminated with 50 Ω impedance.

Figure 10 shows the surface current distribution at 5.72 GHz and 8.66 GHz when all ports are excited. The color field reveals that the current distribution of the proposed four-port MIMO antenna has maximum distribution.

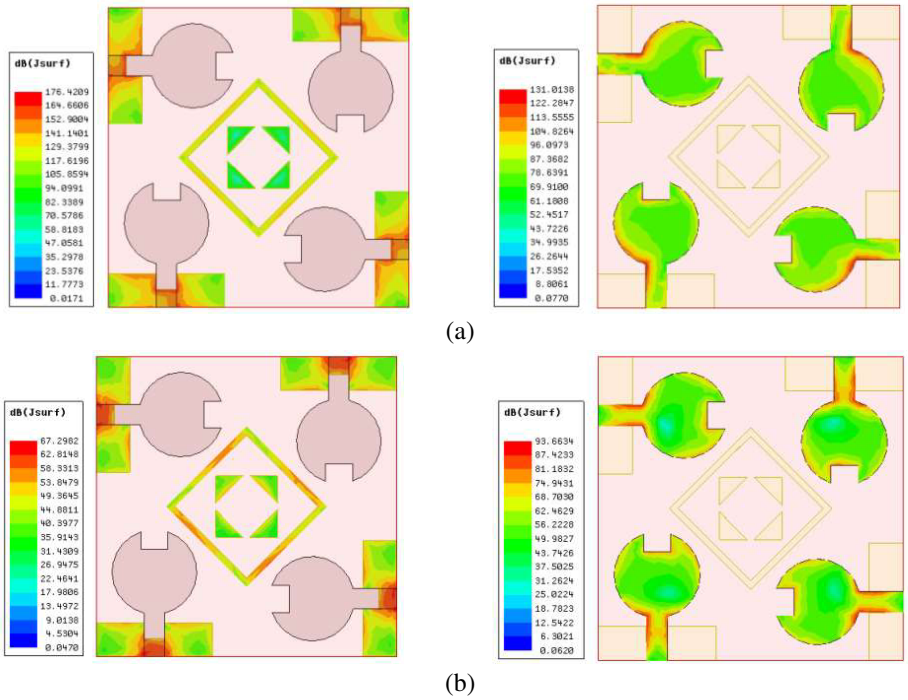

Figure 10. Surface current distributions in ground and top layers of proposed MIMO (a) at 5.72 GHz, (b) at 8.66 GHz.

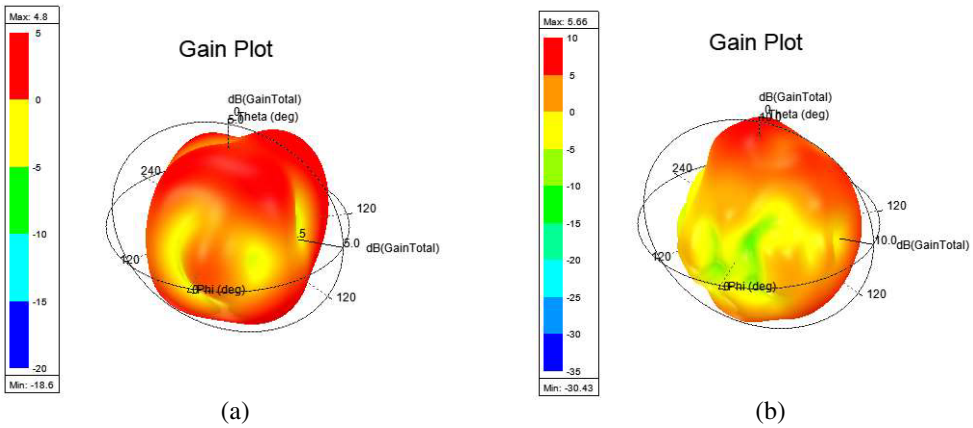

Figure 11. 3D radiation plots of proposed MIMO (a) at 5.84 GHz, (b) at 9.26 GHz.

4.4. Radiation Characteristics

Figure 11 shows the 3D radiation patterns at 5.84 GHz and 9.26 GHz, respectively. The color field reveals that the radiation pattern of the proposed four-port MIMO antenna has maximum radiation.

Figure 12 shows the comparison plots of simulated 2D radiation patterns in XZ, YZ planes for $\phi = 0°$ and $\phi = 90°$, with measured ones at frequencies 5.6 GHz and 8.3 GHz respectively and are in good agreement.

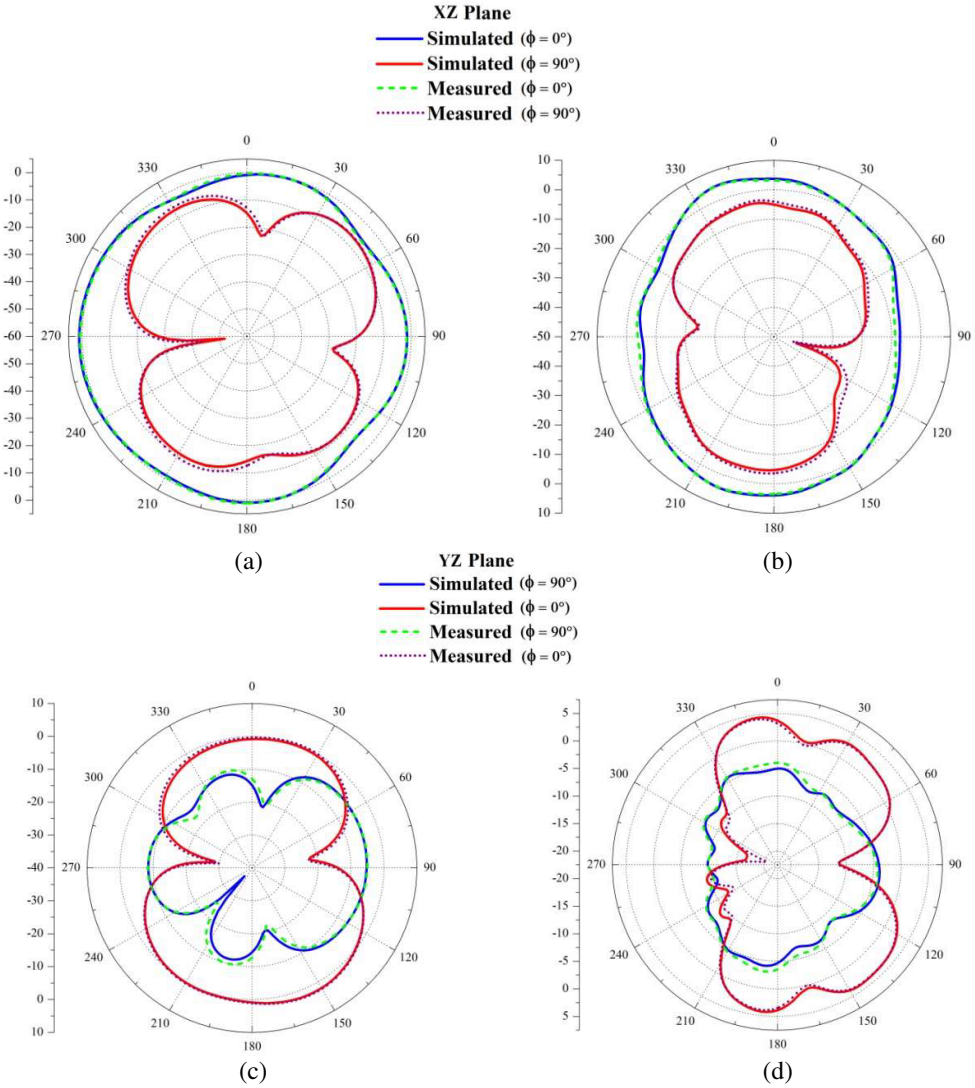

Figure 12. 2D Radiation plots of proposed MIMO design at $\phi = 0°$ and $\phi = 90°$. (a) XZ plane at 5.6 GHz. (b) XZ plane at 8.3 GHz. (c) YZ plane at 5.6 GHz. (d) YZ plane at 8.3 GHz.

4.5. Peak Gain and Radiation Efficiency

Figure 13 shows peak gain and radiation efficiency plots with excited port 1, and the remaining ports are terminated with 50 Ω impedance.

The gain is in the range of 1.27 dBi at 3.1 GHz to 5.15 dBi at 9.2 GHz, and efficiency is in the range of 93% at 6 GHz to 98% at 4.66 GHz. Significantly that the proposed four-port MIMO antenna has gain above 4.5 dBi and efficiency above 96% in the most part of the band of interest 3.1–10.6 GHz.

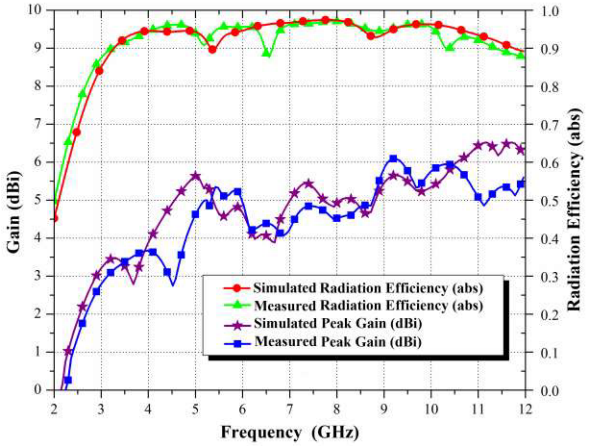

Figure 13. Peak gain and radiation efficiency plots of MIMO antenna.

5. DIVERSITY PERFORMANCE OF PROPOSED FOUR-PORT MIMO ANTENNA

The diversity performance of the proposed four-port MIMO antenna is explained by ECC, DG, TARC, CCL, and MEG. These metrics play a vital role in the characterization of MIMO antennas.

5.1. Measurement of ECC and DG

ECC characterizes the correlation between the jth and ith radiating elements. It is denoted by ρ_{ij}. It is ideally 0, practically less than 0.5. Lower ECC value gives rise to higher isolation, and it leads to good diversity performance. For S parameters, it is expressed by formula (4)

$$ECC = \rho_{ij} = \frac{\left|\sum_{n=1}^{N} S_{in}^{*} S_{nj}\right|^{2}}{\left[1 - \sum_{n=1}^{N} |S_{ni}|^{2}\right]\left[1 - \sum_{n=1}^{N} |S_{nj}|^{2}\right]} \tag{4}$$

where N indicates the number of antenna elements.

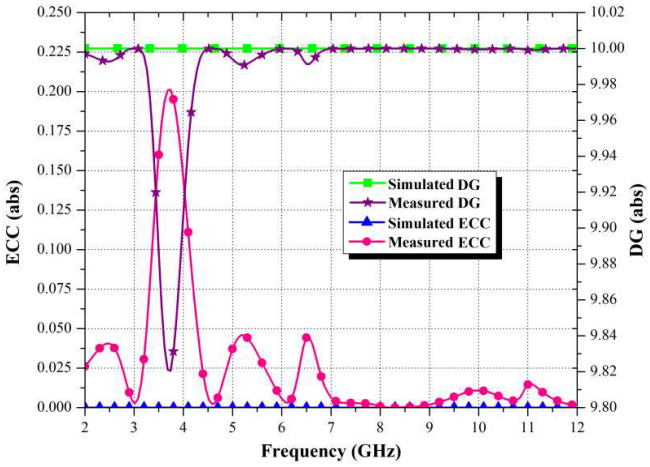

Figure 14. ECC and DG plots of proposed MIMO design.

The objective of diversity is to achieve wideband characteristics with higher isolation between ports. The diversity system is used to measure the degree of correlation. The lower the correlation is, the higher the diversity is. Good diversity gain will be obtained if ECC < 0.5. For a better performance of the MIMO system, DG should be nearly 10 dB, and it is expressed by formula (5)

$$DG = 10\sqrt{1 - ECC^2} \tag{5}$$

Figure 14 shows the proposed four-port MIMO antenna reported as ECC ≤ 0.2, DG ≤ 10, which indicates that ECC and DG are within the permissible limits for 3.1–10.6 GHz, and the measured values closely match the simulated ones.

5.2. Total Active Reflection Coefficient

When all the antenna elements operate in MIMO simultaneously, the efficiency and bandwidth will be affected. So, the TARC is a good one to decide the performance of the MIMO system over S parameters. It is expressed by formula (6).

$$TARC = \sqrt{\frac{Available\ power - Radiated\ power}{Available\ power}} \tag{6}$$

where the sum of powers available at all ports is termed as available power. TARC lies between 0 and 1. If it is 0 that means the total available power is radiated. TARC defines the operating band when all the input signal phases are varied. It is also expressed by formula (7)

$$TARC = \frac{\sqrt{\sum_{i=1}^{4}\left|S_{i1} + \sum_{m=2}^{4} S_{im}e^{j\phi_{m-1}}\right|^2}}{\sqrt{4}} \tag{7}$$

where ϕ = Phase difference between the incoming signals. The accepted value of the TARC in the desired frequency band is < 0 dB. TARC curve must be obtained by keeping the amplitudes of all ports to unity while the excitation phases are varied concerning the first port.

TARC is measured when the input signals of the other three ports are excited with a phase differences between 0° and 180° while keeping the first port constant. From Figure 15 it is observed that TARC ≤ -10 dB for 3.1–10.6 GHz. This indicates low mutual coupling between the ports and ensures stable TARC.

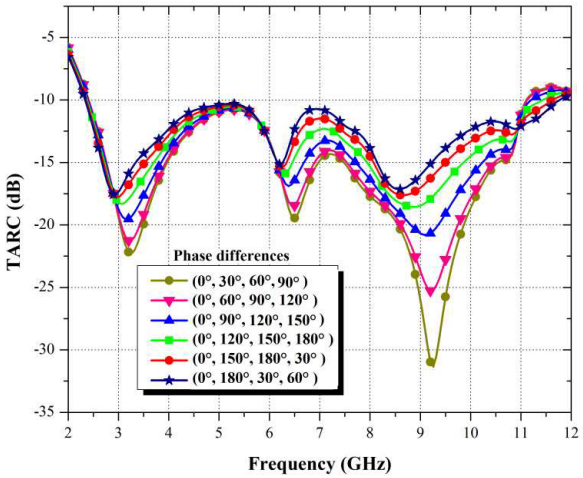

Figure 15. TARC curves of proposed MIMO design.

5.3. Channel Capacity Loss

In a MIMO system without increasing bandwidth or transmitted power levels, the channel capacity increases with the number of radiators. But the interference between elements causes capacity loss. The permissible limit of CCL is 0.4 bits/s/Hz. The CCL for the proposed four-port MIMO antenna is given by formula (8)

$$CCL = -\log_2 det\left(\varphi^R\right) \tag{8}$$

where,

$$\varphi^R = \begin{bmatrix} \rho_{11} & \rho_{12} & \rho_{13} & \rho_{14} \\ \rho_{21} & \rho_{22} & \rho_{23} & \rho_{24} \\ \rho_{31} & \rho_{32} & \rho_{33} & \rho_{34} \\ \rho_{41} & \rho_{42} & \rho_{43} & \rho_{44} \end{bmatrix} \tag{9}$$

$$\rho_{11} = 1 - \left(|S_{11}|^2 + |S_{12}|^2 + |S_{13}|^2 + |S_{14}|^2\right) \tag{10}$$

$$\rho_{12} = -\left(|S_{11}^* S_{12} + S_{12}^* S_{22} + S_{13}^* S_{32} + S_{14}^* S_{42}|\right) \tag{11}$$

$$\rho_{21} = -\left(|S_{21}^* S_{11} + S_{22}^* S_{21} + S_{23}^* S_{31} + S_{24}^* S_{41}|\right) \tag{12}$$

$$\rho_{31} = -\left(|S_{31}^* S_{11} + S_{32}^* S_{21} + S_{33}^* S_{31} + S_{34}^* S_{41}|\right) \tag{13}$$

$$\rho_{44} = 1 - \left(|S_{41}|^2 + |S_{42}|^2 + |S_{43}|^2 + |S_{44}|^2\right) \tag{14}$$

φ^R = Correlation matrix of receiving antenna;
ρ_{ij} = Envelope correlation coefficient;
S_{ii} = Return loss parameter
= The active signal from port i to i;
S_{ji} = Isolation parameter
= Transfer signal from port i to j;
S_{jj} = Return loss parameter at exit port order
= The active signal from port j to j;
S_{ij} = Isolation parameter at exit port order
= Transfer signal from port j to i;
* = Complex conjugate term.

Figure 16 shows that the CCL is ≤ 0.38 bits/s/Hz for 3.1–10.6 GHz and is within the permissible limit.

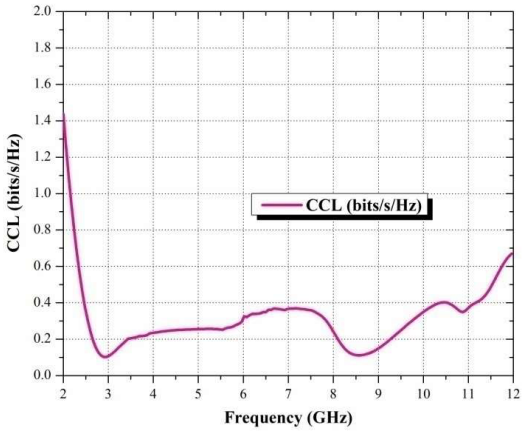

Figure 16. CCL plot of proposed MIMO antenna.

5.4. Mean Effective Gain

MEG is introduced for finding the average strength of the power received from individual antenna elements concerning an isotropic antenna. It is measured usually in a predefined wireless environment. The ratio of MEG between two antennas must be nearly unity for high diversity gain. For S parameters, MEG is expressed by formula (15).

$$MEG_i = 0.5\left[1 - \sum_{j=1}^{N} |S_{ij}|^2\right] \tag{15}$$

Ideally, MEG should be less than -3 dB. The MEG between any two ports must satisfy the condition (16).

$$|MEG_i - MEG_j| < 3\,\text{dB} \tag{16}$$

From Figure 17 the comparison graph ratios of MEG1 to MEG2, MEG3, and MEG4 of the proposed four-port MIMO antenna are near unity, in turn indicating the quality of the design.

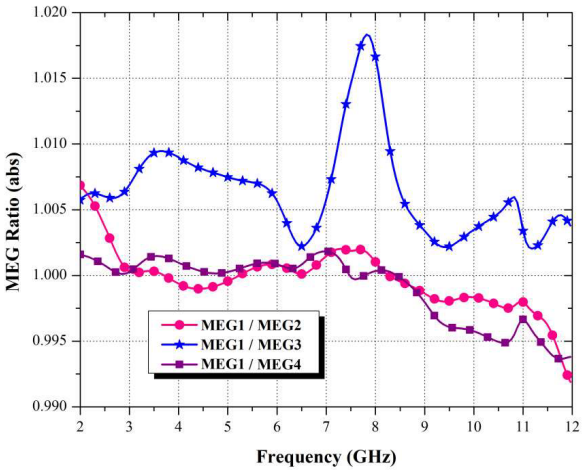

Figure 17. MEG ratio of proposed MIMO.

Table 4. Performance comparison of four-port UWB MIMO antennas.

Ref.	Antenna Size (mm^3)	Substrate	Bandwidth (GHz)	Gain (dBi)	Isolation (dB)	ECC	Radiation Efficiency (%)
[5]	$40 \times 40 \times 1.524$	FR4	3.1–10.6	2.9	< -16	< 0.13	> 90
[7]	$50 \times 50 \times 1.6$	FR4	4.1–14.7	7.23	< -15	< 0.009	NA
[8]	$60 \times 60 \times 1.52$	Taconic TLY 5	3–12.8	6.94	< -21	< 0.001	NA
[18]	$80 \times 80 \times 1.6$	Rogers RT Duroid 5880	3–14	4.8	< -20	< 0.03	> 83
[20]	$50 \times 50 \times 1.6$	FR4	2–12	3.3	< -17	< 0.15	NA
[21]	$45 \times 45 \times 1.6$	FR4	3.1–11	NA	< -16	< 0.015	NA
[24]	$70 \times 41 \times 0.8$	FR4	3.1–12	3.7	< -17	< 0.012	> 80
This Work	**$44 \times 44 \times 1.6$**	**FR4**	**2.33–11.7**	**5.15**	**< -28.24**	**< 0.2**	**> 93**

Table 4 shows the comparison of the proposed four-port MIMO with related UWB MIMOs in the literature. This design indicates low profile, high IBW, very good isolation, high efficiency, and gain with acceptable diversity parameters for 3.1–10.6 GHz. Hence, the proposed four-port MIMO is a good module for cognitive radio applications, as the present-day cognitive radio systems need high gain UWB antenna modules for wideband sensing purposes.

6. CONCLUSION

The paper reports a four-port Wrench-shaped compact UWB MIMO design of size $44 \times 44\,\text{mm}^2$ ($0.342\lambda_0 \times 0.342\lambda_0\,\text{mm}^2$) which is fabricated on an FR4 substrate of thickness 1.6 mm and shows improved isolation by three different novel decoupling structures introduced in the ground plane. This MIMO design has four radiators arranged in an orthogonally symmetric manner. The proposed four-port MIMO design evolution is presented initially with a single element, then four-port MIMO configurations with different inter-element spacings without decoupling structures, and later with three different novel decoupling structures. The design with decoupling structure C in the ground plane achieved optimum results and good diversity performance. Hence, it is finalized for fabrication and measurement results which are in good agreement with the simulated ones. The results are reported as reflection coefficients $S_{11} \leq -10\,\text{dB}$ in the range from 2.33 GHz to 11.7 GHz, mutual coupling coefficients $S_{21} \leq -28.24\,\text{dB}$, $S_{31} \leq -22.35\,\text{dB}$. The maximum peak gain is 5.15 dBi at 9.2 GHz, and the minimum is 1.27 dBi at 3.1 GHz. The maximum efficiency is 98% at 4.66 GHz, and the minimum is 93% at 6 GHz. The diversity parameters are reported as ECC ≤ 0.2, DG ≤ 10, TARC $\leq -10\,\text{dB}$, unity MEG ratio, and CCL $\leq 0.38\,\text{bits/s/Hz}$. This indicates that the proposed four-port UWB MIMO antenna effectively satisfies the necessary MIMO characteristics, and it exhibits good diversity performance concerning ECC, DG, TARC, MEG, and CCL for 3.1–10.6 GHz. This four-port MIMO design is a good module for cognitive radio applications, as the present-day cognitive radio systems need high gain UWB antenna modules for wideband sensing purposes.

REFERENCES

1. Sharawi, M. S., "Printed multi-band MIMO antenna systems and their performance metrics," *IEEE Antennas and Propagation Magazine*, Vol. 55, No. 5, 218–232, 2013.
2. Tiwari, R. N., P. Singh, B. K. Kanaujia, and K. Srivastava, "Neutralization technique based two and four port high isolation MIMO antennas for UWB communication," *AEU-International Journal of Electronics and Communications*, Vol. 110, 152828, Oct. 2019.
3. Nikam, B. V. and M. R. Jadhav, "A compact quad port band-notched MIMO antenna for Wi-Max applications with low mutual coupling," *Progress In Electromagnetics Research C*, Vol. 104, 53–67, 2020.
4. Ali, W. A. E. and A. A. Ibrahim, "A compact double-sided MIMO antenna with an improved isolation for UWB applications," *AEU-International Journal of Electronics and Communications*, Vol. 82, 7–13, Dec. 2017.
5. Singh, D., A. A. Khan, S. A. Naqvi, M. Saeed Khan, A. D. Capobianco, S. Boscolo, M. Midrio, and R. M. Shubair, "Inverted-C ground MIMO antenna for compact UWB applications," *Journal of Electromagnetic Waves and Applications*, 1–14, May 2021.
6. Andrade-González, E. A., J. A. Tirado-Méndez, H. Jardón-Aguilar, M. Reyes-Ayala, A. Rangel-Merino, and M. Pascoe-Chalke, "UWB four ports MIMO antenna based on inscribed Fibonacci circles," *Journal of Electromagnetic Waves and Applications*, 1–19, Jan. 2021.
7. Aggarwal, I., S.a Pandey, M. R. Tripathy, and A. Mittal, "Design and analysis of metamaterial-based SWB-MIMO antenna," *IETE Journal of Research*, 1–14, 2022.
8. Abbas, A., N. Hussain, M. A. Sufian, J. Jung, S. M. Park, and N. Kim, "Isolation and gain improvement of a rectangular notch UWB-MIMO antenna," *Sensors*, Vol. 22, No. 4, 1460, 2022.
9. Rajkumar, S., A. A. Amala, and K. T. Selvan, "Isolation improvement of UWB MIMO antenna utilising molecule fractal structure," *Electronics Letters*, Vol. 55, No. 10, 576–579, Apr. 2019.

10. Desai, A., C. D. Bui, J. Patel, T. Upadhyaya, G. Byun, and T. K. Nguyen, "Compact wideband four element optically transparent MIMO antenna for mm-Wave 5G applications," *IEEE Access*, Vol. 8, 194206–194217, Oct. 2020.
11. Singh, G., S. Kumar, B. K. Kanaujia, and V. K. Pandey, "Design and implementation of a compact tri-band four-port multiple-input-multiple-output antenna," *International Journal of RF and Microwave Computer-Aided Engineering*, e23218, 2022.
12. Keshri, P. K., S. K. Sahu, and R. Chandel, "CSRR-loaded compact quad port MIMO diversity antenna for UWB applications," *IETE Journal of Research*, 1–11, 2021.
13. Wu, Y., W. Wang, W. Wang, and J. Ran, "Design of a tri-band multiple input multiple output antenna with high isolation for 5G applications," *International Journal of RF and Microwave Computer-Aided Engineering*, e23153, 2022.
14. Hasan, Md N., S. Chu, and S. Bashir, "A DGS monopole antenna loaded with U-shape stub for UWB MIMO applications," *Microwave and Optical Technology Letters*, Vol. 61, No. 9, 2141–2149, 2019.
15. Keshri, P. K., R. Chandel, S. Kumar Sahu, and A. K. Gautam, "Compact quad-port high performance UWB MIMO/diversity antenna with slotted ground structure," *Progress In Electromagnetics Research C*, Vol. 112, 193–205, 2021.
16. Tang, Z., X. Wu, J. Zhan, S. Hu, Z. Xi, and Y. Liu, "Compact UWB-MIMO antenna with high isolation and triple band-notched characteristics," *IEEE Access*, Vol. 7, 19856–19865, Feb. 2019.
17. Modak, S., T. Khan, T. A. Denidni, and Y. M. Antar, "Miniaturized self-isolated UWB MIMO planar/cuboidal antenna with dual X-band interference rejection," *AEU-International Journal of Electronics and Communications*, Vol. 143, 154020, 2022.
18. Sadineni, R. B. and P. G. Dinesha, "Design of penta-band notched UWB MIMO antenna for diverse wireless applications," *Progress In Electromagnetics Research M*, Vol. 107, 35–49, 2022.
19. Kulkarni, J., A. Desai, and C.-Y. D. Sim, "Wideband four-port MIMO antenna array with high isolation for future wireless systems," *AEU-International Journal of Electronics and Communications*, Vol. 128, 153507, Jan. 2021.
20. Khan, M. S., A. Iftikhar, R. M. Shubair, A. D. Capobianco, B. D. Braaten, and D. E. Anagnostou, "A four element, planar, compact UWB MIMO antenna with WLAN band rejection capabilities," *Microwave and Optical Technology Letters*, Vol. 62, No. 10, 3124–3131, Oct. 2020.
21. Kumar, S., G. H. Lee, D. H. Kim, W. Mohyuddin, H. C. Choi, and K. W. Kim, "A compact four-port UWB MIMO antenna with connected ground and wide axial ratio bandwidth," *International Journal of Microwave and Wireless Technologies*, Vol. 12, No. 1, 75–85, Feb. 2020.
22. Choudhary, V., M. K. Meshram, and J. Hesselbarth, "Four elements reconfigurable mimo antenna for dual band applications," *International Journal of Advances in Microwave Technology*, Vol. 7, No. 1, 274–282, 2022.
23. Singh, G., S. Kumar, B. K. Kanaujia, and V. K. Pandey, "Design and performance analysis of a frequency reconfigurable four-element multiple-input-multiple-output antenna," *AEU-International Journal of Electronics and Communications*, 154118, 2022.
24. Yang, L., M. Xu, and C. Li, "Four-element MIMO antenna system for UWB applications," *Radioengineering*, Vol. 28, No. 1, 60–67, Apr. 2019.
25. Naktong, W. and A. Ruengwaree, "Four-port rectangular monopole antenna for UWB-MIMO applications," *Progress In Electromagnetics Research B*, Vol. 87, 19–38, 2020.
26. Naidu, P. V., A. Saiharanadh, D. Maheshbabu, A. Kumar, and N. Vummadisetty, "Design and performance analysis of G-shaped compact ACS fed 4-port MIMO antenna for triple frequency band applications," *Progress In Electromagnetics Research C*, Vol. 112, 55–68, 2021.
27. Naidu, P., D. Maheshbabu, A. Saiharanadh, A. Kumar, N. Vummadisetty, L. Sumanji, and K. A. Meerja, "A compact four-port high isolation hook shaped ACS fed MIMO antenna for dual frequency band applications," *Progress In Electromagnetics Research C*, Vol. 113, 69–82, 2021.
28. Islam, S. N. and S. Das, "Isosceles triangular resonator based compact triple band quad element multi terminal antenna," *Radioengineering*, Vol. 29, No. 1, 52–58, Jan. 2020.

29. Saurabh, A. K., P. S. Rathore, and M. K. Meshram, "Compact wideband four-element MIMO antenna with high isolation," *Electronics Letters*, Vol. 56, No. 3, 117–119, 2020.
30. Gayatri, T., G. Srinivasu, D. M. K. Chaitanya, and V. K. Sharma, "Design and analysis of a compact wrench shaped uwb antenna for spectrum sensing in 3.1 GHz to 10.6 GHz," *2020 IEEE International RF and Microwave Conference (RFM)*, 1–4, 2020.